IJIE

The International Journal of Integrated Engineering

Modelling Temperature and Strain-Rate Dependence of Recycled Aluminium Alloy AA6061

C. S. Ho[1], M. K. Mohd Nor[1*], M.S.A. Samad[1, 2]

[1]Crashworthiness and Collisions Research Group (COLORED), Faculty of Mechanical and Manufacturing Engineering, Universiti Tun Hussein Onn Malaysia, Parit Raja, Johor, MALAYSIA

[2]Computer Aided Engineering, Vehicle Performance, Group Research and Development, Perusahaan Otomobil Nasional Bhd (PROTON), Shah Alam, Selangor, MALAYSIA

*Corresponding Author

Abstract: Recycling aluminium is a topic of high interest for numerous researchers to cope with the high demand for usage of its primary sources, and to overcome the environmental issues at the same time. Yet, the deformation behaviour is lacking in the literature and the development of an appropriate numerical analysis of such recycled material is also missing without this information. It is very important to understand the behaviour of the recycled aluminium alloy under various deformation condition before any application is applied. The numerical analysis data is also important for the ease of future application simulation work. Thus, the aim of the present study is to characterize the deformation behaviour of the recycled aluminium alloy under different tensile loading condition and to model a numerical analysis for the prediction of the deformation behaviour of recycled AA6061. The deformation behaviour of the recycled AA6061 was tested over two different loading speed (1.5 mm/min and 15 mm/min) and different elevated temperature (100°C – 300°C). The recycled AA6061 exhibits strain-rate dependence behaviour with mild-ductile-elastoplastic behaviour within the considered loading condition. The degradation of tensile properties is quite significant, which is due to crystallinity. Based on the experimental findings, the material model MAT_098 of Simplified Johnson-Cook model, was adopted and the input parameters were characterized. The simulation results were validated against the experimental data. A good agreement between the experimental and numerical results are obtained. The outcome of numerical analysis is important to prove a strength model is still relevant to predict the deformation behaviour of such recycle material. Further, it showed that further manufacturing advancement is required on the experimental part since an anisotropic parameter are still unavailable, yet vital for consideration.

Keywords: Recycling aluminium alloy, temperature and strain rate dependence, uniaxial tensile test, finite element analysis, LS-DYNA

1. Introduction

In the recent years, recycling aluminium had become exciting topic and many recycling approaches had been established especially solid-state recycling approach, i.e. powder metallurgy [1]–[4], compression method [5], [6], hot extrusion [7]–[11], hot press forging [12]–[15], etc. A promising and satisfactory performance in term of strength is observed comparing to the primary source. However, upon numerous literature review regarding the recycling aluminium, most of the studies are focused on the process setting optimization, the deformation behaviour of such recycled material under different strain rates and elevated temperatures appear to be lacking in the literature. In fact, it is well-known that aluminium alloy are widely adopted in automotive and aerospace application, where it is normally

undergoing different loading condition [16], [17]. Thus, it is crucial to study the deformation behaviour of such recycled material over different loading condition.

It is important to consider a complete response of any material encompass elastoplastic region, rate dependency, and hardening in predicting its behaviour. The response can be anisotropic as a result these factors [18], [19]. Numerous efforts can be seen consider the influence of anisotropic characteristic, which has also attracted attention the user of metal structures including functionally graded natural fiber/epoxy (FGNF/epoxy) [19], [20], [43]. The response is complex since different behaviour is observable in different orientation, compared to isotropic material that has no preferred orientation [40], [41].

The effects of strain rate and temperatures of such material have been investigated using uniaxial tensile test in various works [42], [43]. Interested reader can refer to [22] regarding the mechanical response of aluminium alloy AA2024 and AA5083, while the response of aluminium alloy AA2024 and AA7010 can be found in [23]. In a recycle form of aluminium, the response of hot-extruded recycled AA6061was examined rigorously in [24].

The popularity of the finite element method in predicting material deformation behaviour is increasing in recent years to minimize the cost and time consumption of experiments. It is widely adopted in the prediction of stress-strain behaviour during the structures or components are subjected to mechanical or thermal loading [25], [26]. To study the effects of strain rates and temperatures towards the material behaviour, many strain rate and temperature dependence models, i.e. Johnson-Cook model, Mechanical Threshold Stress (MTS), Zerilli-Armstrong (Z-A), etc., had been published in the previous studies. Many researchers have investigated the flow stress behaviour using numerical analysis to evaluate the influence of strain rates and temperatures [23], [27], [28]. In industrial practice, due to the ability and simplicity in predict the model constants with less effort, the Johnson-Cook model is widely incorporated into most of the numerical simulation tools in modelling the material deformation behaviour efficiently [29].

Murugesan and Jung [29] characterise the flow stress behaviour of AISI-1045 medium carbon steel at elevated temperature and over a range of strain rates using the Johnson-Cook model, including the damage model. The model constants are determined using the experimental data of tensile tests. A good agreement is shown between the experimental and simulation results. Grazka and Janiszewski [30] determine the constants of Johnson-Cook model to predict the deformation behaviour of copper Cu-ETP under Taylor impact test. Explicit solver of ANSYS Autodyn software is used in the numerical analysis. Satisfactory flow behaviour is obtained. As result, the modified Johnson-Cook shows a better and accurate description for predicting the flow stress behaviour of such material under different temperature and strain rate condition. Not only these, Vedantam et al. [31] used Johnson-Cook model for mild and DP steels, Banerjee et al. [32] studied the material response of armour steel using Johnson-Cook model with the Johnson-Cook damage model, Majzoobi and Dehgolan [33] applied Johnson-Cook in their study, etc. A good agreement of the simulation results is obtained in most of the mentioned studies above and the capabilities of the Johnson-Cook model in predicting material deformation behaviour are proved.

In addition, there is also some modification on the Johnson-Cook model is adopted to perform the prediction of material deformation behaviour. Gambirasio and Rizzi [34] implemented Split Johnson-Cook strength model to determine the material behaviour of structural steel, pure metal and stainless steel. The trend of the simulation results is validated against the experimental results. They concluded that the capability of the new strength model in describing the material behaviour is enhanced compare to original Johnson-Cook model. Zhao et al. [35] compare the performance of original Johnson-Cook and modified Johnson-Cook model in predicting dynamic behaviour of laser additive manufacturing FeCr alloy. The modified Johnson-Cook model consider the thermal softening and strain rate hardening effects to overcome the insufficiency of the original Johnson-Cook model. Besides, a simplified Johnson-Cook model is also adopted in the study by Stopel and Skibicki [27] to characterise the material deformation behaviour under Charpy test using LS-DYNA. A satisfactory result is obtained.

Compared with the great number of experimental studies and numerical simulation using the Johnson-Cook model, the prediction of deformation behaviour of the recycled aluminium alloy is still a challenging problem. Based on this motivation, the experimental-numerical analysis in predicting the deformation behaviour of recycled aluminium alloy under quasi-static strain rate ranging from $\times 10^{-4}$ s^{-1} $- \times 10^{-3}$ s^{-1} and elevated temperature of 100 °C, 200 °C, and 300 °C are performed. The model with the least effort in predicting material constants: Johnson-Cook model, is adopted in this study. The simulation results are validated against the experimental results to shows the capability of the finite element method and analysis adopted.

2. Experiment – Uniaxial Tensile Test

Elastic and plastic deformation behaviour can be easily obtained from the stress-strain behaviour of the material. It is vital to provide a better physical understanding associated with material mechanics. Thus, uniaxial tensile test was adopted as one of the characterization tests in this research work, where the mechanical response of recycled AA6061 was examined by performing the finite deformation test of the uniaxial tensile test at various strain rates and temperatures.

2.1 Specimen Preparation

The specimens are processed via hot press forging recycling technique. Further explanation can be found in [34-35]. The optimum process setting for specimen preparation was referred from [36]. Briefly, CNC machine is used to cut the as-received AA6061 into chip using the setting shown in Table 1. Next, the chips were cleaned according to ASTM G131-96, before it was dried in a thermal oven. Later, direct-conversion recycling process is executed using hot press forging process. Next, a heat treatment process was applied to the hot-pressed sample to enhance the strength of the recycled material. The hot-pressed specimen was quenched at 100 °C/s immediately from the hot press forging machine for about five seconds for rapid cooling to room temperature and instantaneous artificial ageing in a 175°C thermal oven for two hours. A specimen undergoing these complete heat-treated processes is denoted as T5-temper. In the present study, ASTM-E21 Standard, which is generally designed for tensile testing at elevated temperatures, was adopted. The specimen's geometry in mm is shown in Fig. 1.

**Table 1 - Chips milling setting [34]**

Parameter	Value
Cutting Speed, v	1100 m/min
Diameter Tool	10 mm
Feed, f	0.05 mm/tooth
Depth of Cut	1 mm
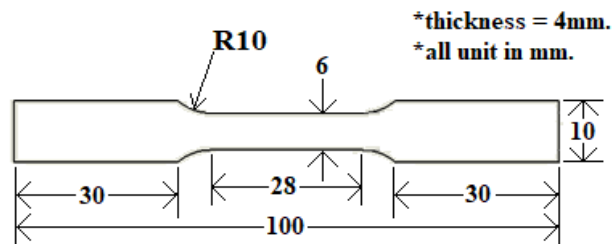
Fig. 1 - ASTM-E21 geometry [34]

2.2 Experimental Procedure

The specimen was tested at elevated temperatures ranging from 100 °C to 300 °C using two loading speeds of 1.5 mm/min and 15 mm/min. The test was performed using Zwick Roell Z030 universal testing machine with attachment of extensometer as shown in Fig. 2. The specimen was pre-heated for about 30 minutes before the tensile test was started.
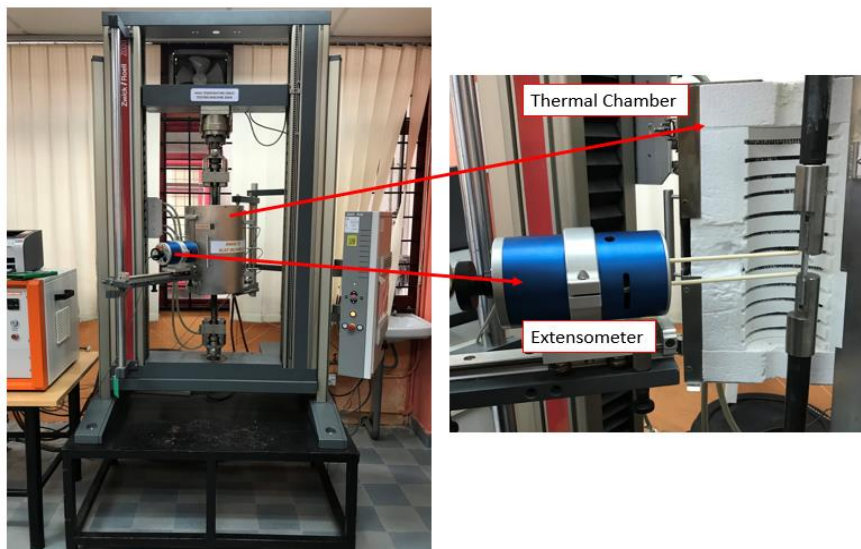
Fig. 2 - Tensile machine with extensometer and thermal chamber

137

2.3 Experimental Results

The strain rate and temperature responses from the uniaxial tensile test data were plotted into stress-strain curves, as shown in Fig. 3. Referring to the curves, flow stress generally increased as strain rate increased. This behaviour is clearly observed at 300 °C, but it is less pronounced at 100 °C and 200 °C. The range of UTS, yield strength, elastic modulus and total elongation at strain rate of 5×10^{-4} s^{-1} were mainly within 189–210 MPa, 153–178 MPa, 62–70 GPa and 2.45%–2.75%, respectively. On the other hand, at strain rate of 5×10^{-3} s^{-1}, the UTS value was within 212–224 MPa, yield strength was within 140–187 MPa, elastic modulus was within 58–70 GPa and total elongation range was within 3.82%–4.54%. UTS value and total elongation were directly proportional to strain rate increases. It is believed that the material required a longer time for energy accumulation at low strain rates, therefore leading to the reduction in strength level [37]. The increase in flow strain with strain rate increases was also due to high dislocation density and the activation of critical resolved shear of non-basal slips system for the material [38].

(a)   (b)
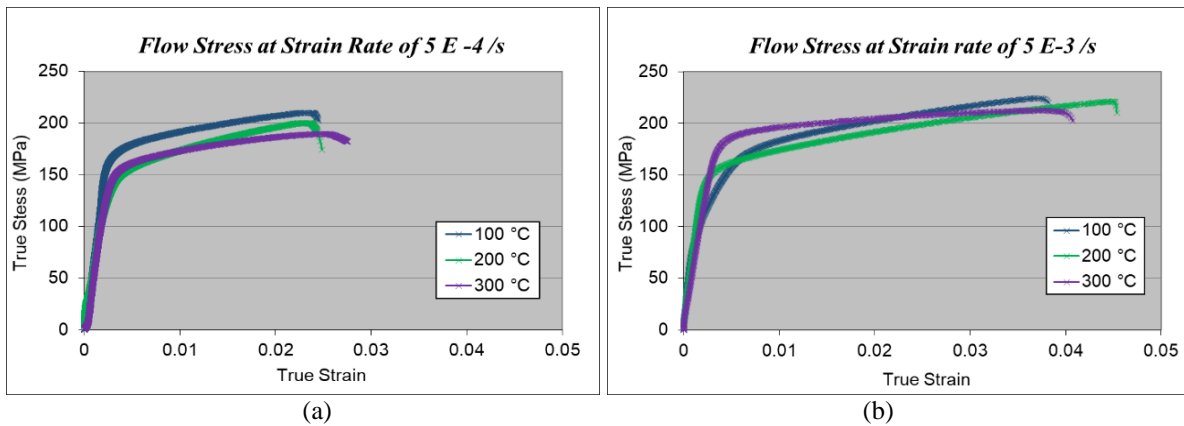
Fig. 3 - Stress-strain curve of recycled AA6061 at strain rate of (a) 5×10^{-4} s^{-1}; (b) 5×10^{-3} s^{-1}

Regarding the total elongation, it can be observed that total elongation to failure at a low strain rate (5×10^{-4} s^{-1}) was smaller compared with a high strain rate (5×10^{-3} s^{-1}). It should be noted that the increase in elongation to failure was affected by strain hardening. Local strain hardening controlled the necking evolution and diffused the necking regions at a high strain rate, resulting in necking getting stronger compared with other regions. Consequently, elongation increased with the increase in strain rate. Generally speaking, it can be accepted that flow stress and total elongation to failure for the recycled material is strain-rate dependent. In other words, the material was capable of sustaining a finite plastic strain deformation without fracture (which indicated good ductility) at a high strain rate compared with a low strain rate at elevated temperature.

Furthermore, as can be seen in Figure 3, there is no specific trend of response towards temperature changes at the beginning of plastic yielding. The trend of flow stress in the plastic region is not consistent with increases in temperature. However, softening effects is observed in the specimen with the increase in temperature in the plastic region, as plastic modulus still existed. In fact, most plastic deformations were transformed into heat, which led to physical ageing and strain softening. Softening effect is normally observed during decreases in stress, as elongation increases upon the onset of yield point. Therefore, it can be accepted in general that flow stress decreased with increasing temperature.

Table 2 compares the mechanical properties between primary form AA6061 obtained from [17] and the recycled form of AA6061 at a strain rate 5×10^{-3} s^{-1} with an elevated temperature of 200 °C. There was about 26% - 27% degradation in the tensile properties of recycled AA6061 compared with the primary form. This is generally due to the change in the microstructure of the recycled AA6061 after undergoing the recycling process. The degradation of ductility a strength properties of the recycled material might be caused by crystallinity. The degree of the crystallinity generally depends on the processing history, such as processing temperature, cooling rate, etc., which could affect the bonding between the chips in the recycled material [39]. In addition, the primary form of AA6061 is reported as strain-rate-dependent and temperature-dependent material, wherein flow stress increases with the strain rate increases and temperature decreases [17]. While recycled AA6061 is sensitive to strain rate changes. The flow stress is slightly decreased with the increment in temperature but there is no specific constant trend is shown at the beginning of the plastic yielding with varying temperature.

**Table 2 - Tensile properties of recycled AA6061 and its primary form**

Material	Recycled AA6061	Primary form AA6061 [17]	Degradation (%)
UTS (MPa)	221.1	299	26.1
Yield Strength (MPa)	158.2	218	27.4
Elastic Modulus (GPa)	70.2	96	26.9

3. Finite Element Analysis

Among numerous strain-rate and temperature dependence models, Johnson-Cook model is widely used in the modelling material deformation behaviour efficiently due to its ability and simplicity in predicting the material constants with less effort [29]. Yet for the Johnson-Cook model, it required a damage model parameter, however, this piece of information is lacking in the existing experimental data. Moreover, there is no specific constant flow stress trend towards the temperature changes at the beginning of the plastic yield. Hence, in the present study, the finite element analysis is performed using material model MAT_098 of Simplified Johnson-Cook model in LS-DYNA, which excluded damage model and temperature dependence is chosen. The explicit dynamic solver is adopted. The following discussed the finite element model and the constitutive model adopted in this work. To validate the finite element analysis, the finite element results is compared with the experimental results.

3.1 Pre-Processing of Finite Element Model

The finite element model is generated according to ASTM-E21 dogbone shape using Solidworks software. The meshing of the model was meshed using the 3D solid map method and quad source shell (square) shape with 0.5 mm of element size. After the meshing work was done, constraints, load, temperature boundary and material model were assigned to the finite element model in the LS-Prepost software. Generally, the finite element model is divided into three main parts, as shown in Fig. 4. The first part is set as a fixed constraint region, where there are no translation and rotation motions within the region during deformation. The second part is the moving constraint region, where force is applied to the region and there are no translation and rotation motions along the y-direction and z-direction. Lastly, the third part is named as deformation region.
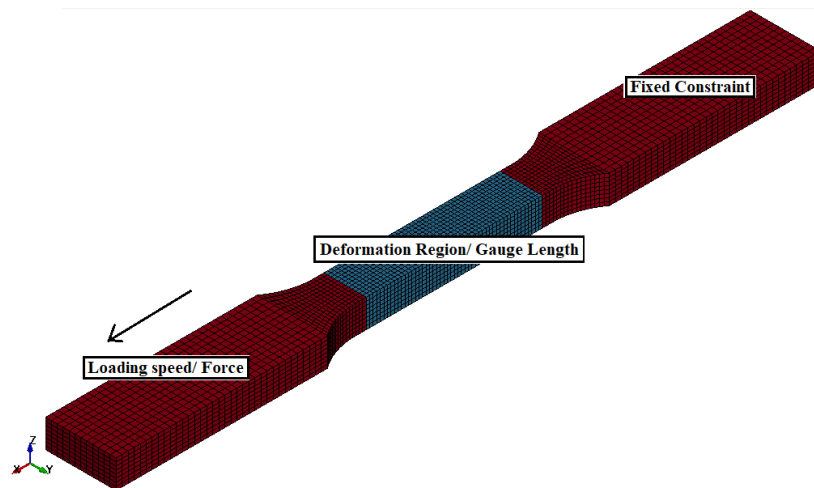
Fig. 4 - Finite element model of uniaxial tensile test

In this research work, temperature boundary was assigned to the finite element model, as the uniaxial tensile tests were performed under elevated temperatures of 100 °C, 200 °C and 300 °C. The constitutive model MAT_098– Simplified Johnson-Cook model in LS-Prepost was allocated to the finite element model using input parameters that were derived specifically for recycled AA6061. The pre-processed finite element model was saved as a keyword format file and was solve using symmetric multiprocessing processor (SMP), a double-precision dynamic solver in LS-DYNA.

3.2 Simplified Johnson-Cook Model

Simplified Johnson-Cook model is simplified from the original Johnson-Cook model by discarding the temperature dependence. The flow stress model is expressed as:

$$\sigma_{eq} = \left[A + B\varepsilon_{pl}^{n} \right]\left[1 + C \ln \dot{\varepsilon}^{*} \right] \tag{1}$$

Here, ε_{pl} represents the effective plastic strain and $\dot{\varepsilon}^{*} = \dfrac{\dot{\varepsilon}}{\dot{\varepsilon}_{0}}$ is the dimensionless strain rate for reference strain rate

($\dot{\varepsilon}_{0}$). A, B, n, and C denote the material input constants. A is the yield stress of the material under reference conditions, B is the strain hardening constant, n is the strain hardening exponent, and C is the strain rate dependence coefficient.

3.2.1 Determination of Material Constants

In this research work, input parameters of the Simplified Johnson-Cook model were derived upon experiment data of the uniaxial tensile test. Reference strain rate was set as 5×10-4 s-1 (loading speed of 1.5 mm/min) for temperatures of 100 °C, 200 °C and 300 °C to perform the data fitting process for the determination of material constants. At this strain rate, the flow stress equation of the Simplified Johnson-Cook model can be simplified as:

$$\sigma_{eq} = \left[A + B\varepsilon_{pl}^{n} \right] \tag{2}$$

Material constants A is equal to stress at zero plastic strain, which can be obtained from experiment data. Based on reference strain rate, material constant A for recycled AA6061 at 100 °C, 200 °C and 300 °C were defined to be 150.56 MPa, 127.54 MPa and 126.90 MPa, respectively.

(a)

(b)

(c)
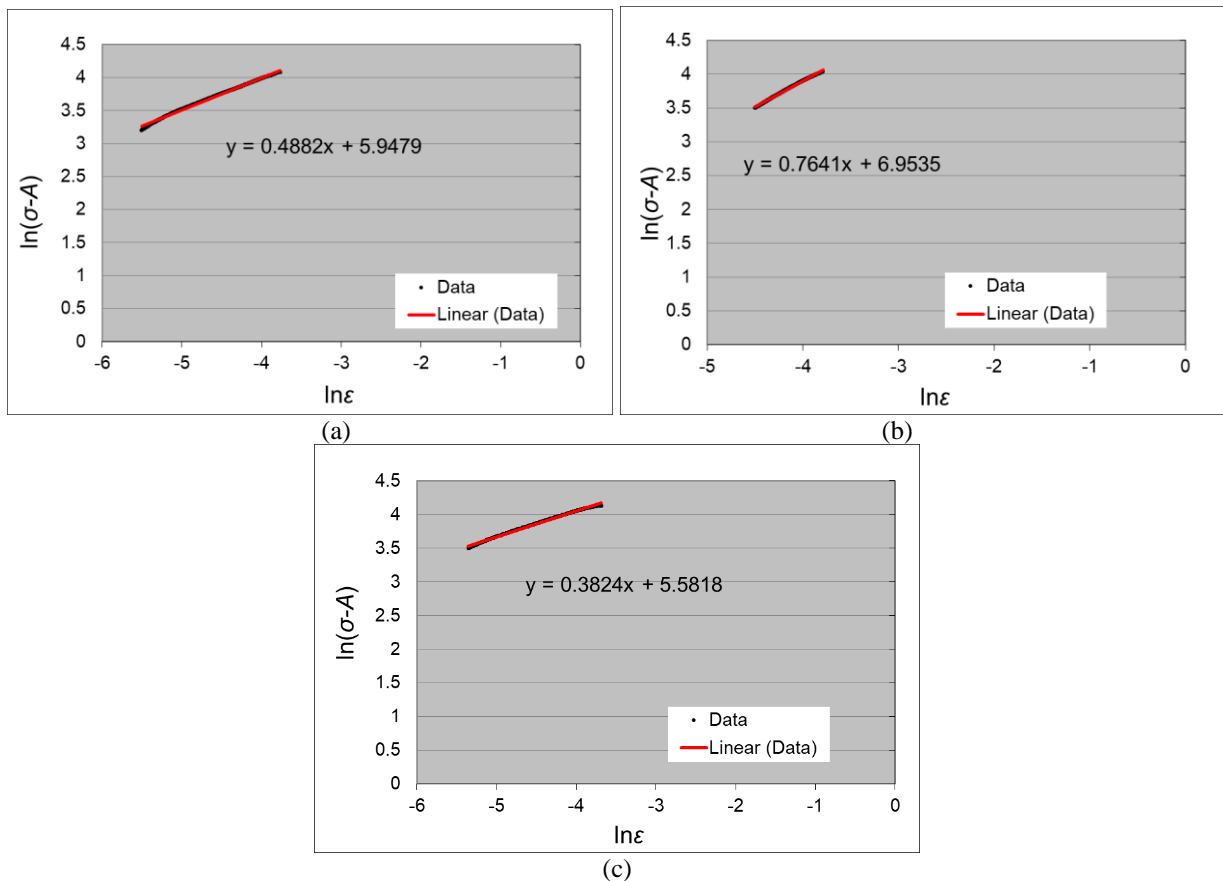
Fig. 5 – Graph of $\ln\left(\sigma_{eq} - A \right)$ **versus** $\ln \varepsilon_{pl}$ **for temperature of (a) 100 °C; (b) 200 °C; (c) 300 °C**

Next, Equation (2) is rearranged into a form of straight-line equation, adding natural logarithm into both sides of the equation, as follows:

$$\ln\left(\sigma_{eq} - A \right) = n \ln \varepsilon_{pl} + \ln B \tag{3}$$

Subsequently, a graph of $\ln\left(\sigma_{eq} - A\right)$ versus $\ln \varepsilon_{pl}$ was plotted, as shown in Fig. 5. Material constant n was represented by the slope of the graph and material constant B was calculated based on the straight-line equation. Material constant B for 100 °C, 200 °C and 300 °C were 382.95 MPa, 793.62 MPa and 265.55 MPa, respectively. On the other hand, material constant n was 0.4882 for 100 °C, 0.6224 for 200 °C and 0.3824 for 300 °C. Furthermore, material constant C was obtained from the graph of $\dfrac{\sigma}{\left[A + B\varepsilon_{pl}^{n}\right]}$ versus $\ln \dot{\varepsilon}^{*}$. The graph can be plotted by rearranging the Simplified Johnson-Cook model into a form of straight-line equation as follows:

$$\frac{\sigma_{eq}}{\left[A + B\varepsilon_{pl}^{n}\right]} = C \ln \dot{\varepsilon}^{*} + 1 \qquad (4)$$

By substituting the obtained values of A, B and n into Equation 4, the graphs of $\dfrac{\sigma}{\left[A + B\varepsilon_{pl}^{n}\right]}$ versus $\ln \dot{\varepsilon}^{*}$ for 100 °C, 200 °C and 300 °C were plotted, as shown in Fig. 6. Material constant C was represented by the slope of the curve, and using the first-order regression model with an intercept value of 1, material constant C for 100 °C, 200 °C and 300 °C were determined to be –0.0404, –0.0103 and 0.0868, respectively.
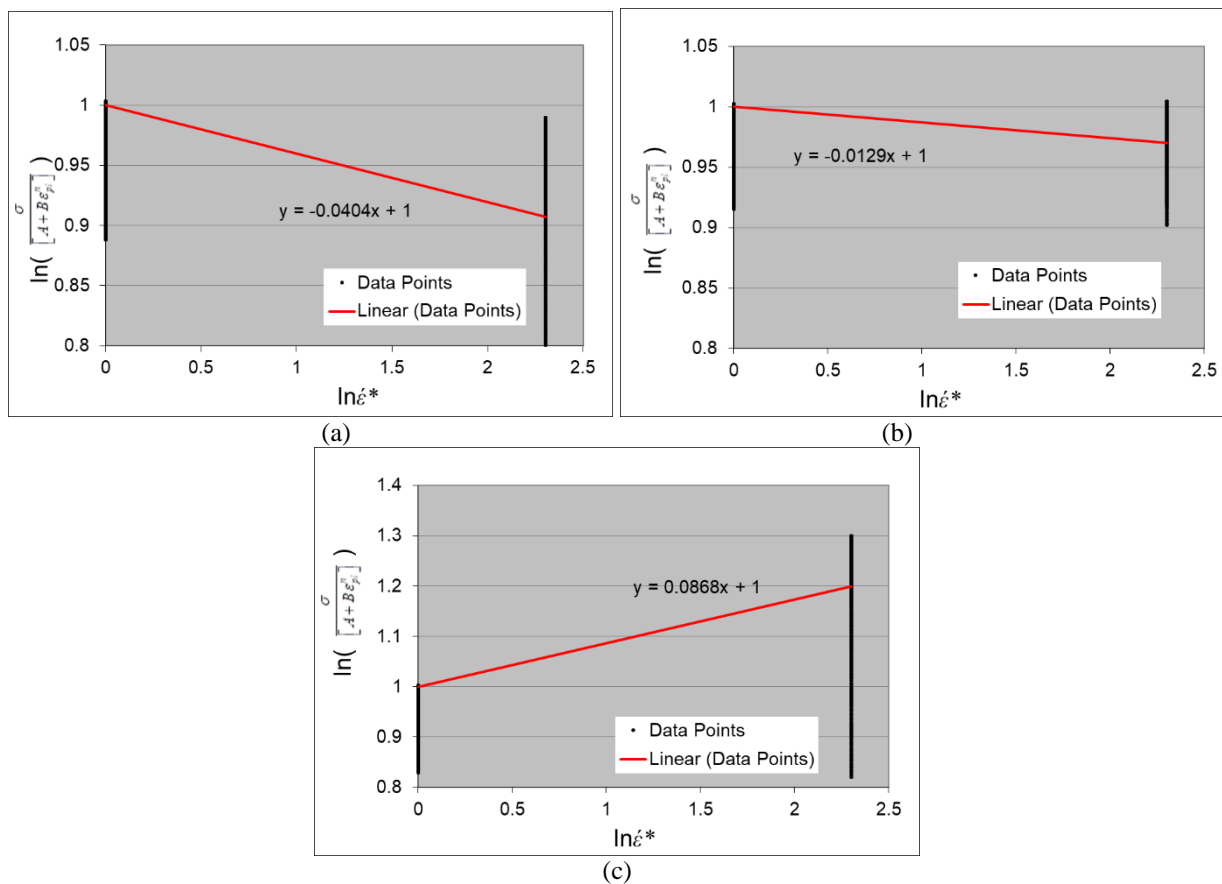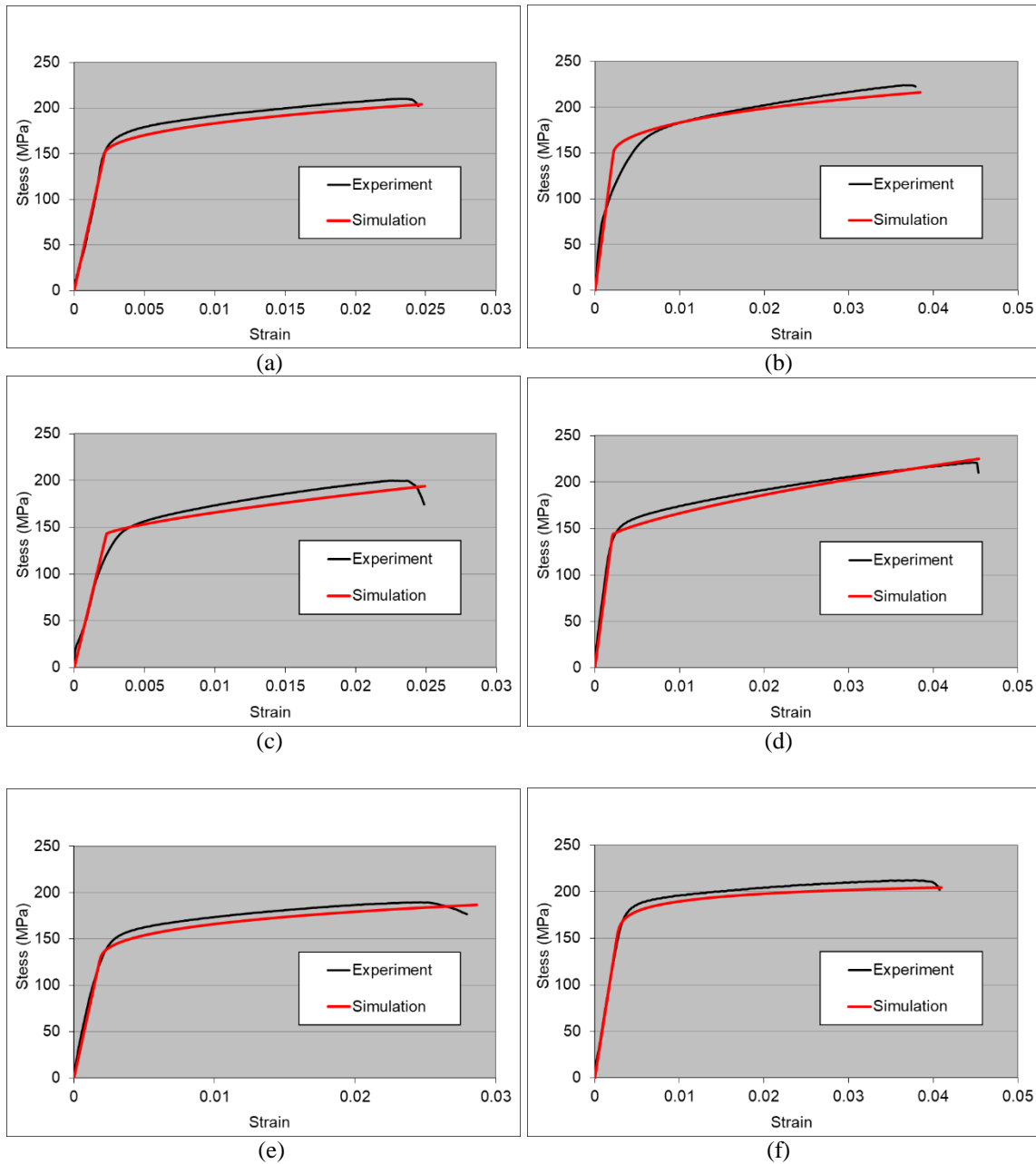

(a)

(b)

(c)

Fig. 6 - Graph of $\dfrac{\sigma}{\left[A + B\varepsilon_{pl}^{n}\right]}$ versus $\ln \dot{\varepsilon}^{*}$ for temperature of (a) 100 °C; (b) 200 °C; (c) 300 °C

3.3 Simulation Results

Fig. 7 illustrates the comparison of the experimental stress-strain curves with the simulation stress-strain curves by using Simplified Johnson-Cook model.

Fig. 7 - Comparison of flow stress curve between simulation result and experimental data (a) 100 °C & 1.5 mm/min; (b) 100 °C & 15 mm/min; (c) 200 °C & 1.5 mm/min; (d) 200 °C & 15 mm/min; (e) 300 °C & 1.5 mm/min; (f) 300 °C & 15 mm/min

From the simulation results, as shown in the figure above, it can be noticed that the flow stress of simulation result showed a good match compared with experiment data. The flow stress of the simulation results show a good match compared to the experimental data. Generally, the Simplified Johnson-Cook model starts flow stress calculation when stress reaches plastic strain, and thus the elastic slope is nearly identical to experiment data. In other words, the formulation of Simplified Johnson-Cook model is starting to be used in the calculation of plastic flow stress from zero plastic strain. From simulation results, the flow stress curve in the plastic region was slightly lower than experiment data. In this simulation work, the finite element model assumed that the area of deformation region was 24 mm² (6mm width × 4mm thick), whereas the thickness of the specimen was about 24 mm² with ±0.5mm tolerance in the actual experiment. Also, the overall percentage errors for yield stress and ultimate tensile strength were lower than 6%, where a percentage error of less than 10% is generally considered acceptable. Therefore, it can be accepted that the flow stress of simulation result was slightly lower compared with experiment result. The comparison of the simulation data and the experimental data are summarized in Table 3.

Table 3 - Simulation result vs experimental data of uniaxial tensile test

Temperature (°C)	Loading Speed (mm/min)	Properties Data	Elastic Modulus, E (GPa)	Yield Strength, σ_{yield} (MPa)	UTS (MPa)
100	1.5	Experiment	70.46	177.64	209.99
		Simulation	69.76	168.14	204.07
		Error (%)	0.97	5.35	2.82
	15	Experiment	69.71	159.20	223.98
		Simulation	69.63	167.80	216.23
		Error (%)	0.11	5.40	3.46
200	1.5	Experiment	62.61	153.83	199.85
		Simulation	62.53	148.95	194.18
		Error (%)	0.13	3.17	2.84
	15	Experiment	69.72	158.21	221.11
		Simulation	69.67	151.46	223.73
		Error (%)	0.07	4.27	1.19
300	1.5	Experiment	69.35	159.27	189.42
		Simulation	69.32	150.72	186.73
		Error (%)	0.04	5.37	1.42
	15	Experiment	57.97	187.39	212.45
		Simulation	57.96	179.80	204.57
		Error (%)	0.02	4.17	3.71

In short, the deformation behaviour of recycled aluminium alloy AA6061 at different tensile loading deformations has been examined. Generally, the adopted constitutive model (MAT_098–Simplified Johnson-Cook model) is capable of predicting the elastoplastic deformation behaviour of recycled AA6061. The input parameters were successfully validated, and a satisfactory agreement was shown in each of the tests when compared with experiment data.

4. Conclusion

In the present study, the deformation behaviour of recycled aluminium alloy AA6061 under uniaxial tensile test at two different strain rates (×10-4 s-1 and ×10-3 s-1) and three elevated temperatures (100°C, 200°C, and 300°C) are evaluated via experimental and numerical analysis. From the experimental work, the effects of strain rate on the recycled AA6061 is clearly observed but there is no specific consistent trend with the changes in temperature at the beginning of plastic yielding. The flow stress and total elongation of the recycled AA6061 are proportional to the increase in strain rate. The increase in total elongation is generally due to the strain hardening effect. In general, experiment works showed the elastoplastic and mild ductile behaviour of recycled AA6061. Based on the experimental findings, the input constants are derived, and a finite element model is modelled, and simulation results were validated against the experiment data. The material model was capable to predicting the deformation of recycled AA6061 and a satisfactory agreement was shown in each simulation test.

Acknowledgement

References

[1] S.-H. Hong, D.-W. Lee, and B.-K. Kim, "Manufacturing of Aluminum Flake Powder from Foil Scrap by Dry Ball Milling Process," J. Mater. Process. Technol., vol. 100, pp. 105–109, 2000.
[2] S. Kumar, F. Mathieux, G. Onwubolu, and V. Chandra, "A Novel Powder Metallurgy-based Method for the Recycling of Aluminum Adapted to a Small Island Developing State in the Pacific," Int. J. Environ. Conscious Des., vol. 13, no. 3,4, pp. 1–22, 2007.

[3] M. Rahimian, N. Parvin, and N. Ehsani, "The Effect of Production Parameters on Microstructure and Wear Resistance of Powder Metallurgy Al–Al2O3 Composite," Mater. Des., vol. 32, no. 2, pp. 1031–1038, 2011.

[4] M. Rahimian, N. Ehsani, N. Parvin, and H. reza Baharvandi, "The Effect of Particle Size, Sintering Temperature and Sintering Time on the Properties of Al-Al2O3 Composites, Made by Powder Metallurgy," J. Mater. Process. Technol., vol. 209, no. 14, pp. 5387–5393, 2009.

[5] B. L. Chan and M. A. Lajis, "Direct Recycling of Aluminium 6061 ChipThrough Cold Compression," Int. J. Eng. Technol., vol. 15, no. 04, pp. 4–8, 2015.

[6] Y. Kume, T. Takahashi, M. Kobashi, and N. Kanetake, "Solid State Recycling of Die-cast Aluminum Alloy Chip Wastes by Compressive Torsion Processing," Keikinzoku/Journal Japan Inst. Light Met., vol. 59, no. 7, pp. 354–358, 2009.

[7] S. N. A. Rahim, M. Z. Mahadzir, N. A. F. N. Abdullah, and M. A. Lajis, "Effect of Extrusion Ratio of Recycling Aluminium AA6061 Chips by the Hot Extrusion Process," Int. J. Adv. Res. Eng. Innov., vol. 1, no. 2, pp. 15–20, 2019.

[8] A. Ahmad, M. A. Lajis, and N. K. Yusuf, "On the Role of Processing Parameters in Producing Recycled Aluminum AA6061 Based Metal Matrix Composite (MMC-AlR) Prepared using Hot Press Forging (HPF) Process," Materials (Basel)., vol. 10, no. 9, pp. 1–15, 2017.

[9] M. Haase and A. E. Tekkaya, "Recycling of Aluminum Chips by Hot Extrusion with Subsequent Cold Extrusion," in Procedia Engineering, 2014, vol. 81, pp. 652–657.

[10] S. N. A. Rahim, M. A. Lajis, and S. Ariffin, "Effect of Extrusion Speed and Temperature on Hot Extrusion Process of 6061 Aluminum Alloy Chip," ARPN J. Eng. Appl. Sci., vol. 11, no. 4, pp. 2272–2277, 2016.

[11] A. E. Tekkaya, M. Schikorra, D. Becker, D. Biermann, N. Hammer, and K. Pantke, "Hot Profile Extrusion of AA-6060 Aluminum Chips," J. Mater. Process. Technol., vol. 209, no. 7, pp. 3343–3350, 2009.

[12] N. K. Yusuf, M. A. Lajis, and A. Ahmad, "Multiresponse Optimization and Environmental Analysis in Direct Recycling Hot Press Forging of Aluminum AA6061," Materials (Basel)., vol. 12, no. 12, pp. 1–25, 2019.

[13] M. A. Lajis, A. Ahmad, N. K. Yusuf, A. H. Azami, and A. Wagiman, "Mechanical Properties of Recycled Aluminium Chip Reinforced with Alumina (Al2O3) Particle," Materwiss. Werksttech., vol. 48, no. 3, pp. 306–310, 2017.

[14] S. S. Khamis, M. A. Lajis, and R. A. O. Albert, "A Sustainable Direct Recycling of Aluminum Chip (AA6061) in Hot Press Forging Employing Response Surface Methodology," Procedia CIRP, vol. 26, pp. 477–481, 2015.

[15] A. Ahmad, M. A. Lajis, and N. K. Yusuf, "On the Role of Processing Parameters in Producing Recycled Aluminum AA6061 Based Metal Matrix," Materials (Basel)., vol. 10, no. 1098, pp. 1–15, 2017.

[16] C. S. Ho, M. A. Ab Rani, M. K. Mohd Nor, N. Ma'at, M. T. Hameed Sultan, M. A. Lajis, N. K. Yusuf, "Characterization of Anisotropic Damage Behaviour of Recycled Aluminium Alloys AA6061 Undergoing High Velocity Impact," Int. J. Integr. Eng., vol. 11, no. 1, pp. 247–256, 2019.

[17] N. Ma'at, M. K. M. Nor, and C. S. Ho, "Effects of Temperature and Strain Rate on the Mechanical Behaviour of Commercial Aluminium Alloy AA6061," J. Adv. Res. Fluid Mech. Therm. Sci., vol. 54, no. 1, pp. 21–26, 2019.

[18] T. A. I. De Vuyst, "Hydrocode Modelling of Water Impact," Cranfield University: PhD Thesis, 2003.

[19] M. K. M. Nor, "Modeling of Constitutive Model to Predict the Deformation Behaviour of Commercial Aluminum Alloy AA7010 Subjected to High Velocity Impacts," ARPN J. Eng. Appl. Sci., vol. 11, no. 4, pp. 2349–2353, 2016.

[20] M. K. M. Nor, N. Ma'at, C. S. Ho, and M. S. A. Samad, "An Anisotropic Deformation Analysis of Orthotropic Materials subjected to High Velocity Impacts," Int. J. Mech. Mechatronics Eng., vol. 17, no. 5, pp. 156–172, 2017.

[21] A. Gavrus and H. Francillette, "An Anisotropic Behaviour Analysis of AA2024 Aluminium Alloy Undergoing Large Plastic Deformations," in Aluminium Alloys, Theory and Applications, InTech Open, 2011, pp. 49–68.

[22] M. K. M. Nor and I. M. Suhaimi, "Effects of Temperature and Strain Rate on Commercial Aluminum Alloy AA5083," Appl. Mech. Mater., vol. 660, pp. 332–336, 2016.

[23] V. Panov, "Modelling of Behaviour of Metals at High Strain Rates," Ph.D. Thesis, Cranfield University, 2006.

[24] S. K. Y. Alaric, "Material Characterization of Recycled Aluminium Alloy (AA6061) undergoing Finite Strain Deformation," Universiti Tun Hussein Onn Malaysia, 2017.

[25] A. E. Ismail, S. Jamian, K. Kamarudin, M. K. M. Nor, M. N. Ibrahim, and M. A. Choiron, "An Overview of Fracture Mechanics with ANSYS," Int. Jounal Integr. Eng. Spec. Issue 2018, vol. 10, no. 5, pp. 59–67, 2018.

[26] M. K. M. Nor, N. Ma'at, and C. S. Ho, "An Anisotropic Elastoplastic Constitutive Formulation Generalised for Orthotropic Materials," Contin. Mech. Thermodyn., vol. 30, no. 7, pp. 1–36, 2018.

[27] M. Stopel and D. Skibicki, "Determination of Johnson-Cook Model Constants by Measurement of Strain Rate by Optical Method," AIP Conf. Proc., vol. 1780, no. 06003, pp. 1–9, 2016.

[28] B. Banerjee, "The Mechanical Threshold Stress Model for Various Tempers of AISI 4340 Steel," Int. J. Solids Struct., vol. 44, no. 3–4, pp. 834–859, 2007.

[29] M. Murugesan and D. W. Jung, "Johnson Cook Material and Failure Model Parameters Estimation of AISI-1045 Medium Carbon Steel for Metal Forming Applications," Materials (Basel)., vol. 12, no. 4, pp. 1–18, 2019.

[30] M. Grązka and J. Janiszewski, "Identification of Johnson-Cook Equation Constants using Finite Element Method," Eng. Trans., vol. 60, no. 3, pp. 215–223, 2012.

[31] K. Vedantam, D. Bajaj, N. S. Brar, and S. Hill, "Johnson - Cook Strength Models for Mild and DP 590 Steels," AIP Conf. Proc., vol. 845 I, no. June, pp. 775–778, 2006.

[32] A. Banerjee, S. Dhar, S. Acharyya, D. Datta, and N. Nayak, "Determination of Johnson Cook Material and Failure Model Constants and Numerical Modellng of Charpy Impact Test of Armour Steel," Mater. Sci. Eng. A, vol. 640, pp. 200–209, 2015.

[33] G. H. Majzoobi and F. R. Dehgolan, "Determination of the Constants of Damage Models," Procedia Eng., vol. 10, pp. 764–773, 2011.

[34] L. Gambirasio and E. Rizzi, "An Enhanced Johnson-Cook Strength Model for Splitting Strain Rate and Temperature Effects on Lower Yield Stress and Plastic Flow," Comput. Mater. Sci., vol. 113, pp. 231–265, 2016.

[35] Y. Zhao, J. Sun, J. Li, Y. Yan, and P. Wang, "A Comparative Study on Johnson-Cook and Modified Johnson-Cook Constitutive Material Model to Predict the Dynamic Behavior Laser Additive Manufacturing FeCr Alloy," J. Alloys Compd., vol. 723, no. June 2017, pp. 179–187, 2017.

[36] N. K. Yusuf, M. A. Lajis, and A. Ahmad, "Hot Press as a Sustainable Direct Recycling Technique of Aluminium: Mechanical Properties and Surface Integrity," Materials (Basel)., vol. 10, no. 8, p. 902, 2017.

[37] R. Bobbili, V. Madhu, and A. K. Gogia, "Tensile Behaviour of Aluminium 7017 Alloy at Various Temperatures and Strain Rates," J. Mater. Res. Technol., vol. 5, no. 2, pp. 190–197, 2016.

[38] N. A. Latif, Z. Sajuri, and J. Syarif, "Effect of Tensile Strain Rates on Flow Stress for Extruded AZ31 and AZ61 Magnesium Alloys," Int. J. Automot. Mech. Eng., vol. 14, no. 1, pp. 3812–3823, 2017.

[39] G. Wypych, "Recycling," in Handbook of Material Weathering, 6th ed., Canada: ChemTec Publishing, 2018, pp. 851–861.

[40] AE Ismail, SH Masran, S Jamian, KA Kamarudin, MK Mohd Nor, NH Muhd Nor, AL Mohd Tobi, MK Awang (2016), Fracture Toughness of Woven Kenaf Fibre Reinforced Composites, IOP Conf. Ser.: Mater. Sci. Eng. 160 012020.

[41] M. K. Mohd Nor, C. S. Ho, N. Maat, M. F. Kamarulzaman (2020) Modelling Shock Waves In Composite Materials Using Generalised Orthotropic Pressure, Continuum Mech. Thermodyn. 32, 1217–1229 (2020).

[42] Norzarina Maat, Mohd Khir Mohd Nor, Choon Sin Ho, Noradila Abdul Latif, Al Emran Ismail, Kamarul-Azhar Kamarudin, Saifulnizan Jamian, Mohd Norihan Ibrahim@Tamrin , Muhamad Khairudin Awang (2019), Effects Of Temperatures And Strain Rate On The Mechanical Behaviour Of Commercial Aluminium Alloy AA6061, Journal Of Advanced Research in Fluid Mechanics and Thermal Sciences, Penerbit Akademia Baru, 1, 21, ISSN:22897879

[43] Ho, C.S., Mohd Nor, M.K. (2021) An Experimental Investigation on the Deformation Behaviour of Recycled Aluminium Alloy AA6061 Undergoing Finite Strain Deformation. Met. Mater. Int. 27, 4967–4983. https://doi.org/10.1007/s12540-020-

[44] Maximus Kohnizio Mahli, Saifulnizan Jamian, Al Emran Ismail, Nik Hisyamudin Muhd Nor, M K Mohd Nor, Kamarul Azhar Kamarudin (2018) Effect of Rotating Mold Speed on Microstructure of Al LM6 Hollow Cylinder Fabricated Using Centrifugal Method, J. Phys.: Conf. Ser. 1049 012042